

Supplementary Information

Electrocatalytic C-C Coupling of CO₂ and Formaldehyde to Synthesize Acetate via Membrane Electrode Assembly

Shaohan Xu,^a Jingui Zheng,^a Lingzhi Sun,^a Xun Pan,^a Ruochen Yang,^a Jianrong Zeng,^{b,c} and Guohua Zhao^{a,}*

^a School of Chemical Science and Engineering, Shanghai Key Lab of Chemical Assessment and Sustainability, Tongji University, Shanghai 200092, China.

^b Shanghai Synchrotron Radiation Facility, Shanghai Advanced Research Institute, Chinese Academy of Sciences, Shanghai 201204, China.

^c Shanghai Institute of Applied Physics, Chinese Academy of Sciences, Shanghai 201800, China.

Corresponding Author

*Guohua Zhao, E-mail: g.zhao@tongji.edu.cn

Experimental section

Synthesis of Cu₂O nanoparticles

Cu₂O was synthesized as a supported catalyst by a typical process.¹ 5 mL of 0.5 M CuCl₂·2H₂O aqueous solution was mixed with 5 mL of 5 M NaOH solution under magnetic stirring. After stirring for 30 min, 5 mL of 0.5 M glucose solution was added into the above suspension. Afterward, the reaction was kept at 50 °C until the suspension turns brick red. The products were collected by centrifugation and rinsed with deionized (DI) water and ethanol for three times.

Synthesis of MOF-coated Cu₂O (Cu₂O@MOF) nanoparticles

The Cu₂O supported Cu-MOF core-shell nanoparticles were prepared via a solvothermal reaction.² 16 mg of HHTP ligands were dissolved into 8 mL of *N,N*-dimethylformamide (DMF), forming solution A. 20 mg of the as-prepared Cu₂O nanoparticles were dispersed in 32 mL of DMF and 1200 μL DI water under ultrasonication for 30 min, forming solution B. Subsequently, solution A and B were mixed in a flask and reacted for 10 min at 120 °C in oil bath. The Cu₂O@MOF catalysts were collected by centrifugation and rinsed with DMF and methanol for three times. The obtained sample was dried in a vacuum oven at 60 °C overnight.

Synthesis of Cu-MOF nanoparticles

Cu-MOF nanoparticles were prepared for comparison experiments.² 10 mg of Cu(CH₃COO)₂·H₂O were dissolved in 5 mL of DMF and 1 mL of DI water. Then, 12 mg of HHTP ligands were dissolved into 5 mL of DMF to form homogeneous solution, which was added to the above solution under stirring. The mixed solution was heated in an oil bath and kept at 120 °C for 2 hours. The Cu-MOF powder was collected via centrifugation followed by being rinsed with DMF and DI water for three times and dried in a vacuum oven at 60 °C overnight.

Preparation of IrO_x/Ti mesh anode

Ti mesh loaded with IrO_x catalysts was fabricated via a dip coating and thermal decomposition method.³ Ti mesh was washed with acetone, ethanol and DI water respectively by ultrasonication, and then etched for 1h in boiling 0.5 M oxalic acid. Afterward, the processed Ti mesh was dip coated in 10 mL isopropanol mixed with 10 vol% HCl dissolving 30 mg IrCl₃·xH₂O, which was followed by drying at 60°C and calcination at 500°C for 10 min under

air atmosphere. This process was repeated until a catalyst mass loading of 1 mg cm^{-2} was achieved.

Material characterization

The crystal structure of the prepared catalysts was characterized by X-ray diffraction (XRD, D8 Focus X-ray diffractometer, Bruker, Germany), and the chemical states of catalysts were tested by X-ray photoelectron spectroscopy (XPS, AXIS Ultra DLD). Extended X-ray absorption fine structure (EXAFS) spectra of $\text{Cu}_2\text{O}@$ MOF were obtained on the BL13SSW beamline at the Shanghai Synchrotron Radiation Facility (SSRF).

Co-electrolysis in MEA electrolyzer

4 mg of the catalyst was dispersed in 200 μL of ethanol, 200 μL of DI water and 20 μL of Nafion by ultrasound for 1 h. Subsequently, the as-prepared ink was dropped onto the carbon paper ($2 \times 2 \text{ cm}$) to acquire GDE with a loading mass of 1 mg cm^{-2} . The performances of electrochemical CO_2 and HCHO coupling to produce acetate by $\text{Cu}_2\text{O}@$ MOF were investigated on a Princeton Applied Research potentiostat (Model 263A) at room temperature ($25 \text{ }^\circ\text{C}$). The customized membrane electrode assembly electrolyzer was composed of two pieces of titanium plate equipped with a serpentine flow field of $2 \times 2 \text{ cm}$. The prepared electrode and IrO_x/Ti mesh were employed as the cathode and anode respectively. The cathode and anode were separated by an anion-exchange membrane (AEM, FAA-PK-130, Fumasep). 1 M KOH was employed as the anolyte and circulated by a peristaltic pump at a flow rate of 10 mL min^{-1} . CO_2 gas flowed in a humidifier containing HCHO solution, and then together with gaseous HCHO were fed into the cathode at a flow rate of 30 sccm. The outlet of cathode chamber was connected to a gas/liquid separator which contains pure DI water.

Co-electrolysis in H-cell

Aqueous co-electrolysis of CO_2 and HCHO was conducted in a traditional H-type cell where the cathode and anode were separated by Nafion-117 proton exchange membrane. The electrochemical experiments were conducted on an electrochemical workstation (CHI660, Chenhua Corp., China) with a three-electrode system. The working electrode was $\text{Cu}_2\text{O}@$ MOF on carbon paper ($1 \times 1 \text{ cm}$) with a loading of 1 mg cm^{-2} . The counter and reference electrodes were Pt plate and saturated calomel electrode (SCE) respectively. CO_2 was purged into the catholyte containing HCHO for at least 30 min prior to electrochemical experiments so as to

ensure CO₂ saturation. Linear sweep voltammetry (LSV) polarization curves were measured in CO₂-saturated formaldehyde-containing KOH solution with a sweep rate of 50 mV s⁻¹. The double-layer capacitance (C_{dl}) was obtained by recording cyclic voltammograms with different scan rates to evaluate the electrochemical active surface areas (ECSAs).

Gas-chromatography analysis

The concentration of gas-phase products was monitored online using a gas chromatography (GC-2014C, Shimadzu, Japan, H₂ and N₂ carrier) equipped with a thermal conductivity detector for H₂ detection, a flame ionization detector for C₂H₂, C₂H₄ and C₂H₆ detection, and a methanizer for CO and CH₄ detection. During constant potential electrolysis, effluent gas from the working compartment was injected into the sampling loop of the gas-chromatography (1 mL).

¹H Nuclear magnetic resonance analysis

NMR spectroscopy was employed to quantify the yield of liquid products, such as acetate, methanol, formate and other compounds generated during constant potential electrolysis. ¹H NMR spectra of the liquid products were recorded on a Bruker AVANCE-HD 600 MHz NMR station using dimethyl sulfoxide (DMSO) as an internal standard. 700 μL of liquid sample was mixed with 35 μL of internal standard solution for NMR measurements. The internal standard solution was prepared by mixing 3 ml of D₂O with 2 μL of DMSO. The standard curve for each product was constructed by the relative peak area ratio of the product to DMSO.

The detection of HCHO in the electrolyte solution after the reaction was performed by a reported method.⁴ The sample of HCHO was mixed with a 1 M NaHSO₃ solution (50:50, v/v) and stirred vigorously to form sodium formaldehyde bisulfite adduct, which gives a singlet peak at ~4.39 ppm (with water set at 4.8 ppm) in the ¹H NMR spectra.

In-situ infrared spectroscopy measurements

The in-situ electrochemical infrared spectra were acquired via an infrared spectrometer (Nicolet 8700, Thermo Fisher Scientific Inc., USA). The applied potential was adjusted by a Chenhua CHI660 electrochemical workstation. In-situ measurements were performed under external reflection mode, employing a customized quartz four-neck reactor with a CaF light window as the electrochemical cell. 4 mg of the as-prepared Cu₂O@MOF powder was ultrasonically dispersed in 420 μL ink consisting of DI water, ethanol and Nafion with a volumetric ratio of

10:10:1. 20 μL of the obtained ink was dropped onto a glassy carbon electrode, which was then dried for an hour. The glassy carbon electrode coated with catalyst, platinum wire (0.1 mm) and saturated calomel electrode were employed as the working, counter and reference electrodes respectively. The glassy carbon electrode was placed perpendicular to the CaF light window to minimize the effect of water during the test. In 10 mL of CO_2 -saturated 1 M KOH solution containing HCHO, the in-situ electrochemical infrared spectra were monitored with the real-time variation of applied potential. Chronoamperometry was performed and simultaneously collected spectral signals during electrolysis, and all spectra were background-subtracted and baseline-calibrated.

In-situ Raman measurements

The in-situ Raman experiments were conducted by a confocal Raman microscope (inVia, Renishaw) and the laser excitation source is 532 nm. The instrument was calibrated using silicon wafers (520.5 cm^{-1}) prior to the tests. The experiments were performed in a homemade single-chamber Teflon electrochemical cell with a circular quartz light window. The carbon paper with 1 mg/cm^2 catalyst loading, platinum sheet and saturated calomel electrode were employed as the working, counter and reference electrodes, respectively. The electrochemical experiments were performed in 5 mL of CO_2 -saturated 1 M KOH solution containing 0.1 M HCHO, and the applied potential was modulated by the CHI660 electrochemical workstation. In the experiments, the 532 nm laser source was focused vertically onto the surface of the working electrode through a $50\times$ objective lens.

Online differential electrochemical mass spectrometry (DEMS) measurements

CO_2 -saturated 1 M KOH solution containing HCHO was circulating into a customized electrochemical cell by a peristaltic pump. A graphite electrode sheet coated with catalysts, a platinum gauze electrode, and a saturated calomel electrode were used as the working electrode, the counter electrode and the reference electrode, respectively. The cathode and anode were separated by Nafion-117 proton exchange membrane. The mass signals were recorded under electrochemical potentiostatic mode at the optimal potential of -1.4 V vs. SCE. After the mass signal returned to baseline by switching off the potential, the next cycle started under the same test conditions for a total of four cycles to avoid the accidental error. Notably, the DEMS signal with a m/z value of 28 can be assigned to the fragment ions from both CO and the reactant CO_2 . The CO signal intensity was obtained by subtracting the portion contributed by CO_2 according

to the following equation:

$$i(\text{CO}) = i(m/z = 28) - 6.5/100 * \Delta i(m/z = 44)$$

where i denotes the DEMS signal intensity, 6.5/100 is the ratio of the signal intensity at m/z values of 28 and 44 contributed by CO_2 measured in this DEMS system, and $\Delta i(m/z=44)$ is the change in signal intensity of $m/z=44$, which is negative due to the consumption of CO_2 during the reaction. For sole CO_2 and HCHO electroreduction, the process was the same except that the feeding solution was replaced with CO_2 -saturated 1 M KOH and 1 M KOH solution containing HCHO, respectively.

X-ray absorption fine spectroscopy (XAFS) experiments

All XAFS experiments were conducted at SSRF (BL13SSW beamline) using fluorescence mode for data collection. In situ XAFS was collected using an electrochemical in situ fluorescence X-ray absorption spectroscopy reaction cell made from polyetheretherketone (PEEK). The Kapton tape was employed as a light window to allow the fluorescence detector with 45° X-ray acquisition. A three-electrode system was used for the experiments, in which the catalyst ink was loaded on one side of the working electrode ($1.5 \times 1.5 \text{ cm}^2$ carbon paper) and close to light window to minimize the effect of water during the measurements. 30 mL of 1 M KOH containing 0.1 M HCHO was used as electrolyte, and CO_2 was purged continuously for at least 30 minutes to saturation before electrolysis. X-ray absorption near edge structure (XANES) spectra were calibrated to the characteristic absorption edge of Cu foil. The Fourier transformed k^3 -weighted extended X-ray absorption fine structure (EXAFS) spectra were obtained using Athena without phase correction.

Computational methods

All the density functional theory (DFT) calculations were conducted using the Vienna Ab Initio Package (VASP)^{5,6} within the PBE generalized gradient approximation (GGA)⁷ formulation. The projected augmented wave (PAW) potentials^{8,9} were utilized to describe the ionic cores and valence electrons were considered using a plane wave basis set with an energy cutoff of 450 eV. The Gaussian smearing method with a spread width of 0.05 eV was used to allow the partial occupancies of the Kohn-Sham orbitals. The on-site corrections (DFT+U) was applied to the 3d electrons of Cu atoms ($U_{\text{eff}} = 6.0 \text{ eV}$) via the approach reported by Dudarev et al.¹⁰ The electronic energy is regarded self-consistent when the energy change is smaller than 10^{-5} eV, and geometry optimization is regarded convergent when the force change is smaller than

0.02 eV/Å. The dispersion interactions were described using Grimme's DFT-D3 methodology¹¹.

The lattice constant of the cubic Cu₂O unit cell was optimized to be $a=4.246$ Å. We then used it to construct a Cu₂O(111) surface model (model 1) with p (4×4) periodicity in the X and Y directions and two stoichiometric layers in the Z direction with a vacuum depth of 15 Å. Model 1 consists of 128 Cu and 64 O atoms. Model 2 was built by loading a Cu-MOF cluster onto the surface of Model 1. The structural optimization of the model was carried out by using the Γ point in the Brillouin zone for k-point sampling and fixing the bottom stoichiometric layer while leaving the rest of the atoms fully relaxed.

The adsorption energy (E_{ads}) of adsorbate A was defined as:

$$E_{ads} = E_{A/surf} - E_{surf} - E_{A(g)}$$

where $E_{A/surf}$, E_{surf} and $E_{A(g)}$ are the energy of adsorbate A adsorbed on the material surface, the energy of clean material surface, and the energy of isolated A molecule in a cubic periodic box with a side length of 20 Å and a 1×1×1 Monkhorst-Pack k-point grid for Brillouin zone sampling, respectively. A negative value of E indicates that the adsorption is an exothermic process.

The free energy of gaseous molecules and surface adsorbates is calculated by the equation $G = E + ZPE - TS$, where E is the total energy, ZPE is the zero-point energy, T is the temperature in Fahrenheit (currently 298.15 K is used), and S is the entropy.

Supplementary Figures and Tables

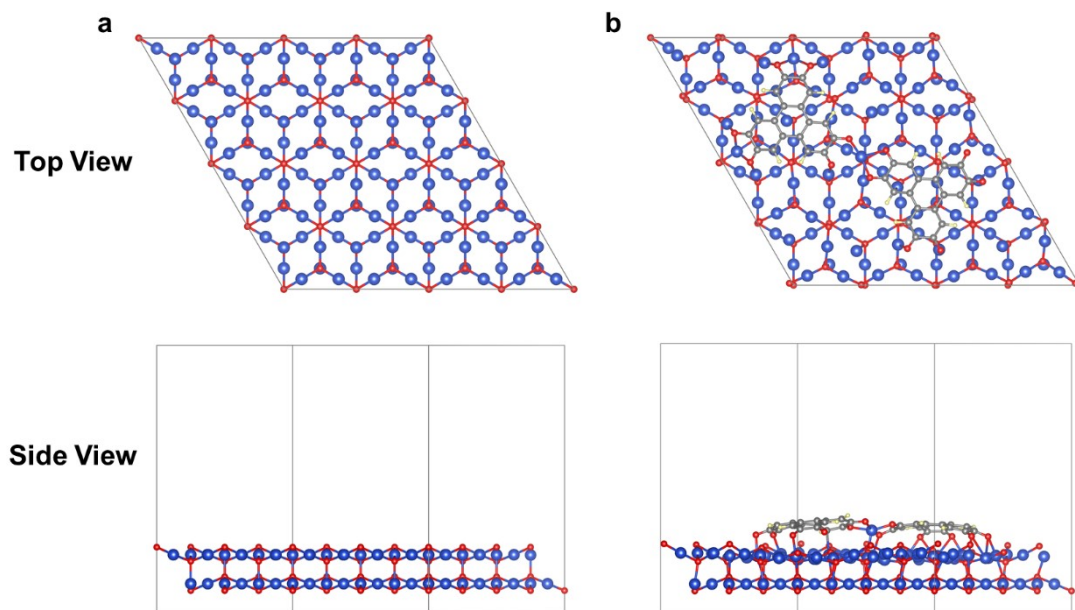


Fig. S1 The top view (above) and side view (below) of optimized structure for a) Cu_2O and b) $\text{Cu}_2\text{O}@$ MOF. Color codes: Cu, blue; O, red; C, grey; H, yellow.

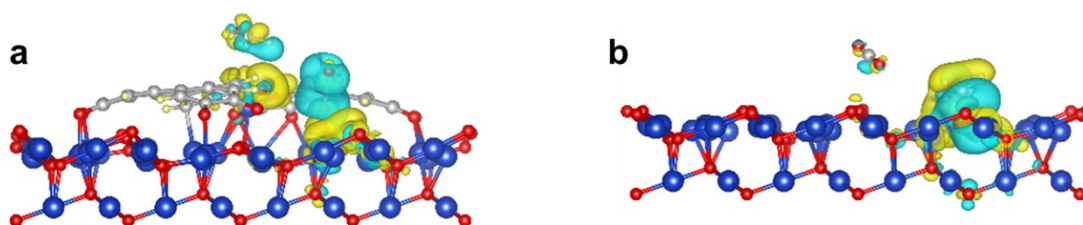


Fig. S2 Side-view of charge density difference analysis for a) $\text{Cu}_2\text{O}@$ MOF and b) Cu_2O with the cyan region representing charge depletion and the yellow region representing charge accumulation.

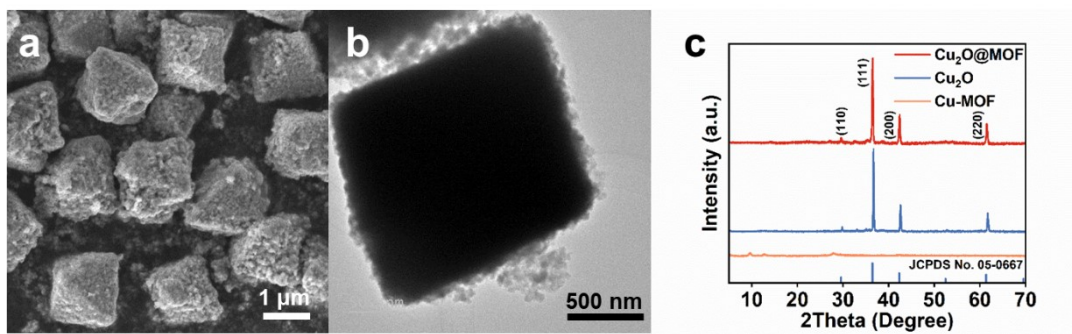


Fig. S3 a) SEM, b) TEM images and c) XRD patterns of $\text{Cu}_2\text{O}@$ MOF.

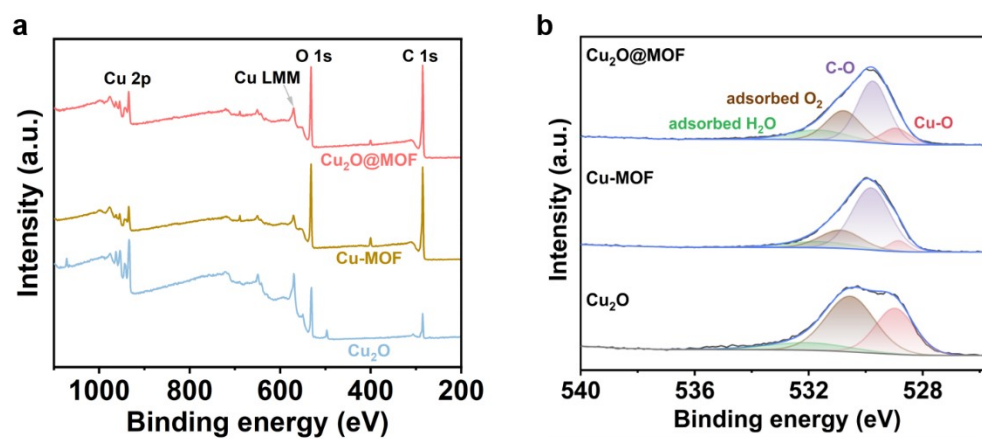


Fig. S4 XPS characterization of Cu_2O , Cu-MOF and $\text{Cu}_2\text{O}@$ MOF. a) XPS survey spectrum and b) O 1s spectra.

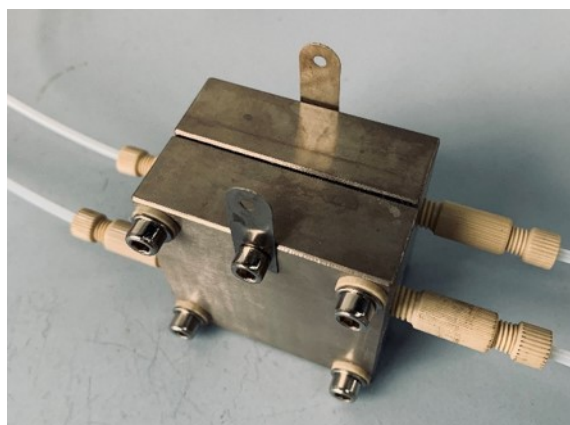


Fig. S5 Photo of the zero-gap membrane electrode assembly electrolyzer.

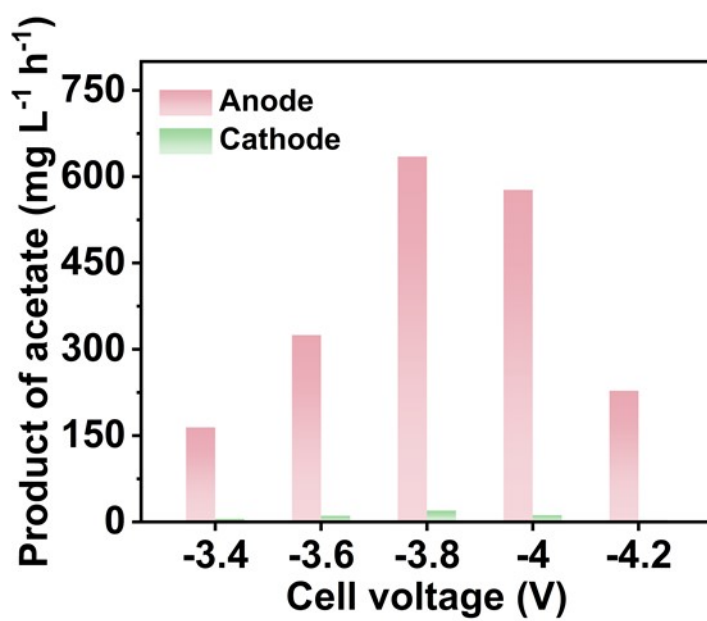


Fig. S6 Amounts of acetate production that are collected from the anode and cathode stream at different cell voltages.

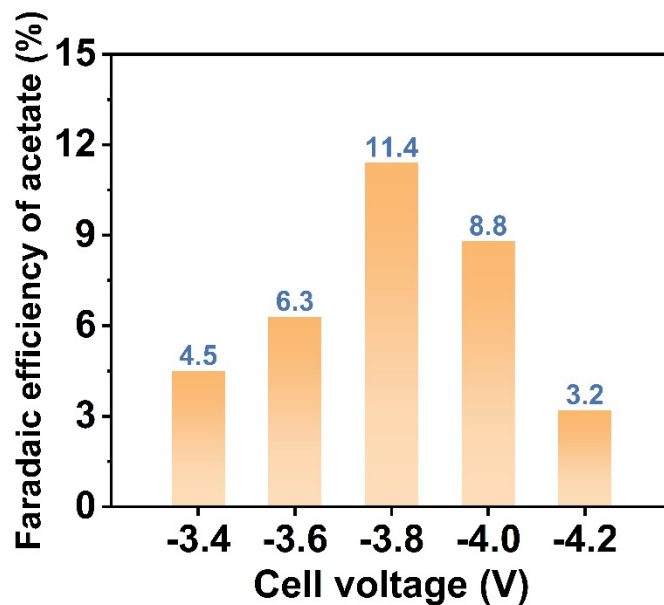


Fig. S7 Faradaic efficiency of acetate product under different cell voltages on Cu₂O@MOF in MEA electrolyzer. For liquid products, the Faradaic efficiency is the percentage of the partial electric charge (Q(product)) in the total charge (Q(total)) passed, which is calculated as follows:

$$\text{Faradaic efficiency (\%)} = \frac{Q(\text{product})}{Q(\text{total})} \times 100\% = \frac{n(\text{product}) \times z \times F}{Q(\text{total})} \times 100\%$$

Where n(product) (mol) is the content of liquid product generated; z is the number of electrons required for the target product, and z=4 for acetate produced from CO₂ and HCHO coupling; F denotes the Faraday constant, which is 96485 C mol⁻¹; Q(total) (C) is the total amount of charge passed.

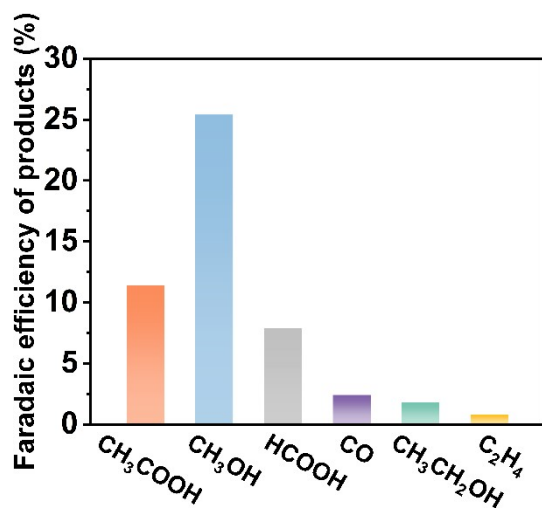


Fig. S8 Faradaic efficiency of different products on Cu₂O@MOF in MEA electrolyzer.

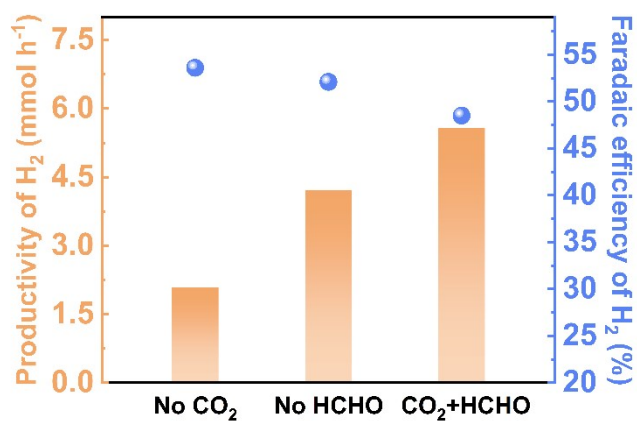


Fig. S9 Productivity and Faradaic efficiency of hydrogen in the presence of different reactants at a cell voltage of -3.8 V on Cu₂O@MOF in MEA electrolyzer.

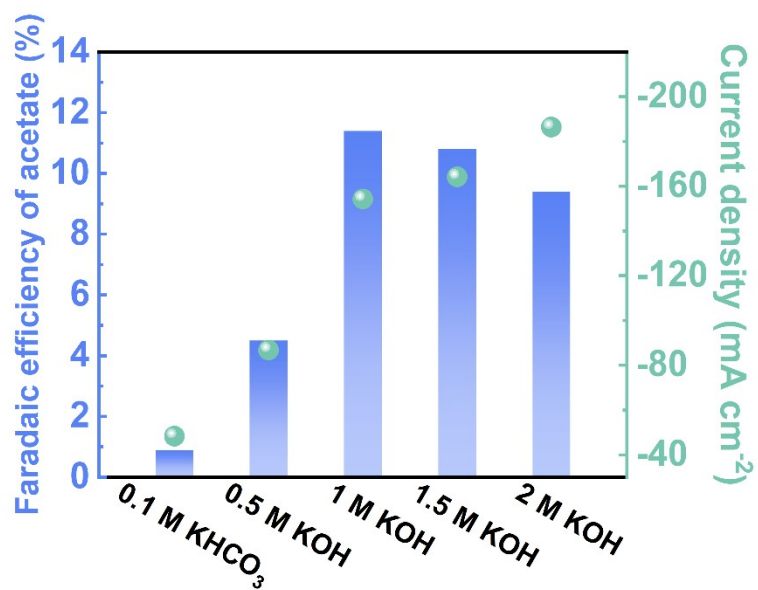


Fig. S10 Faradaic efficiency of acetate and current density with different analytes in MEA electrolyzer.

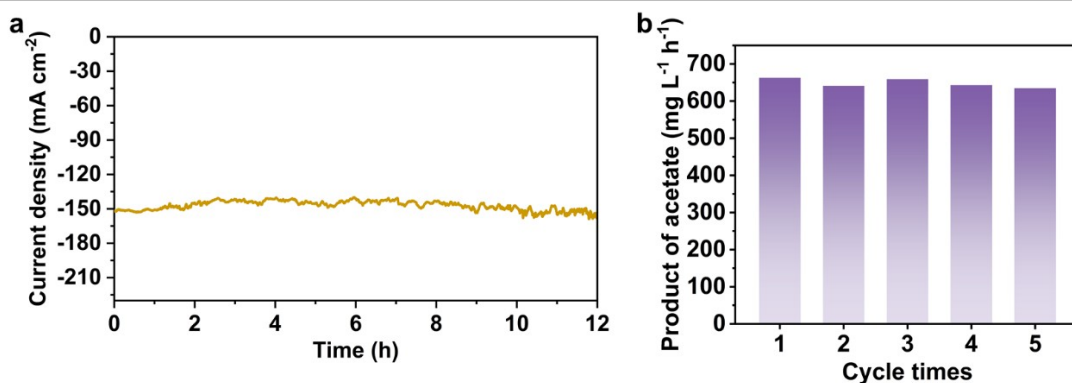


Fig. S11 a) Chronoamperometric i-t curve over Cu₂O@MOF at a cell voltage of -3.8 V for 12-hour continuous co-electrolysis of CO₂ and HCHO in MEA electrolyzer. b) The acetate production over Cu₂O@MOF with two-hour electrolysis at a cell voltage of -3.8 V in MEA electrolyzer under five consecutive cycles.

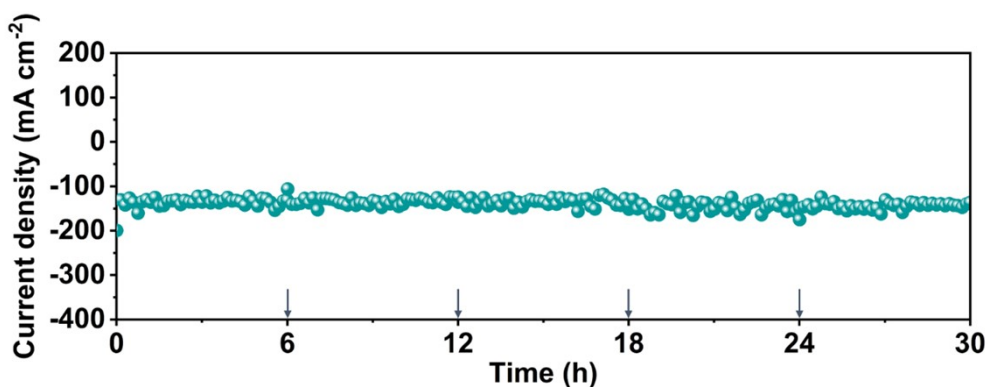


Fig. S12 The long-term stability of CO₂ and HCHO co-electrolysis on the Cu₂O@MOF catalyst at a cell voltage of -3.8 V in MEA electrolyzer. The vertical arrow marks the time of refreshing the electrolyte.

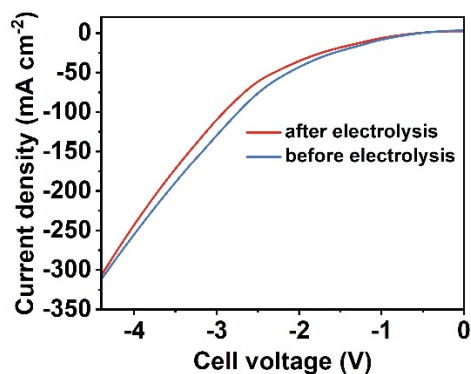


Fig. S13 LSV curves of Cu₂O@MOF in MEA electrolyzer before and after electrolysis.

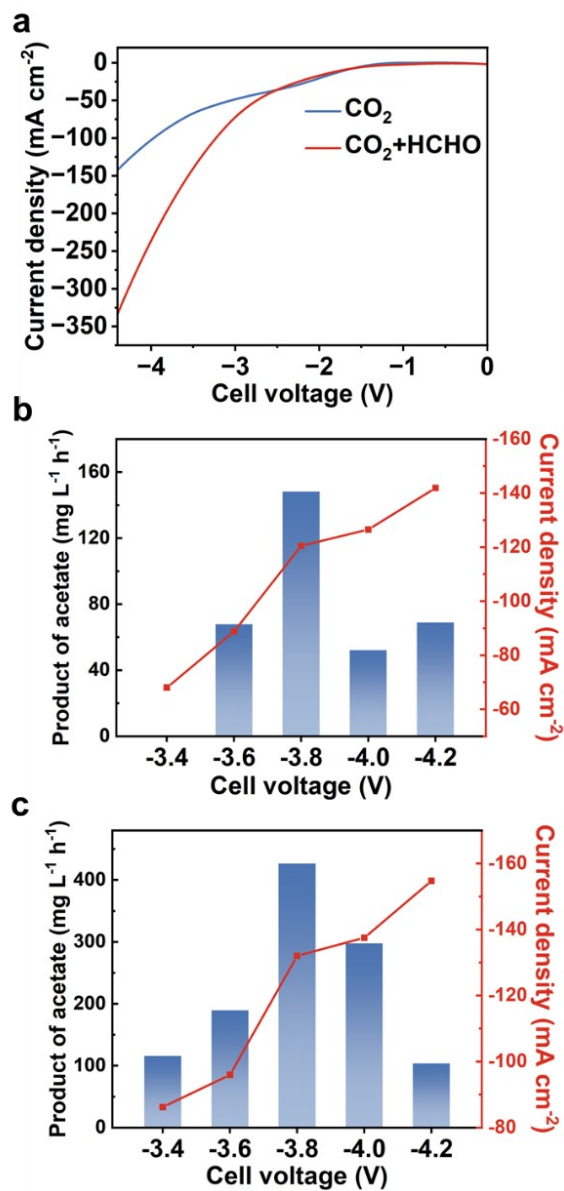


Fig. S14 a) LSV curves of $\text{Cu}_2\text{O@MOF}$ in the presence and absence of formaldehyde. Production rate of acetate and current density under different cell voltages on b) Cu-MOF and c) Cu_2O .

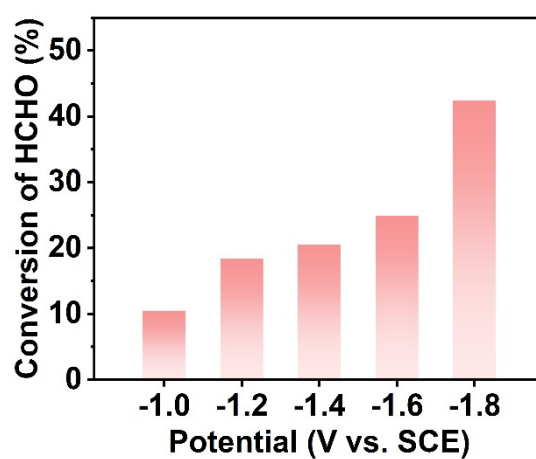


Fig. S15 The conversion of HCHO at different potentials in H-type cell, which is calculated according to the following equation:

$$\text{Conversion (\%)} = \frac{\text{mole of HCHO consumed}}{\text{mole of HCHO initial}} \times 100\%$$

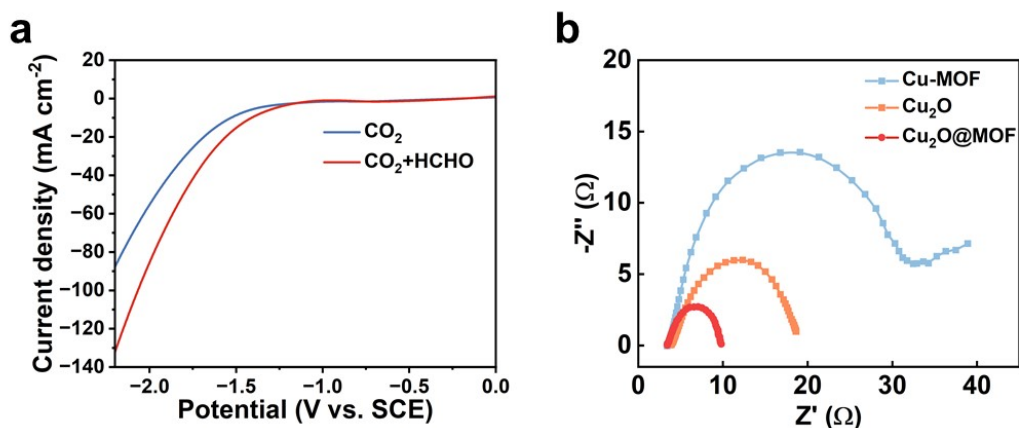


Fig. S16 a) LSV curves of $\text{Cu}_2\text{O}@MOF$ in the presence and absence of formaldehyde in H-type cell. b) EIS of Cu_2O , Cu-MOF and $\text{Cu}_2\text{O}@MOF$.

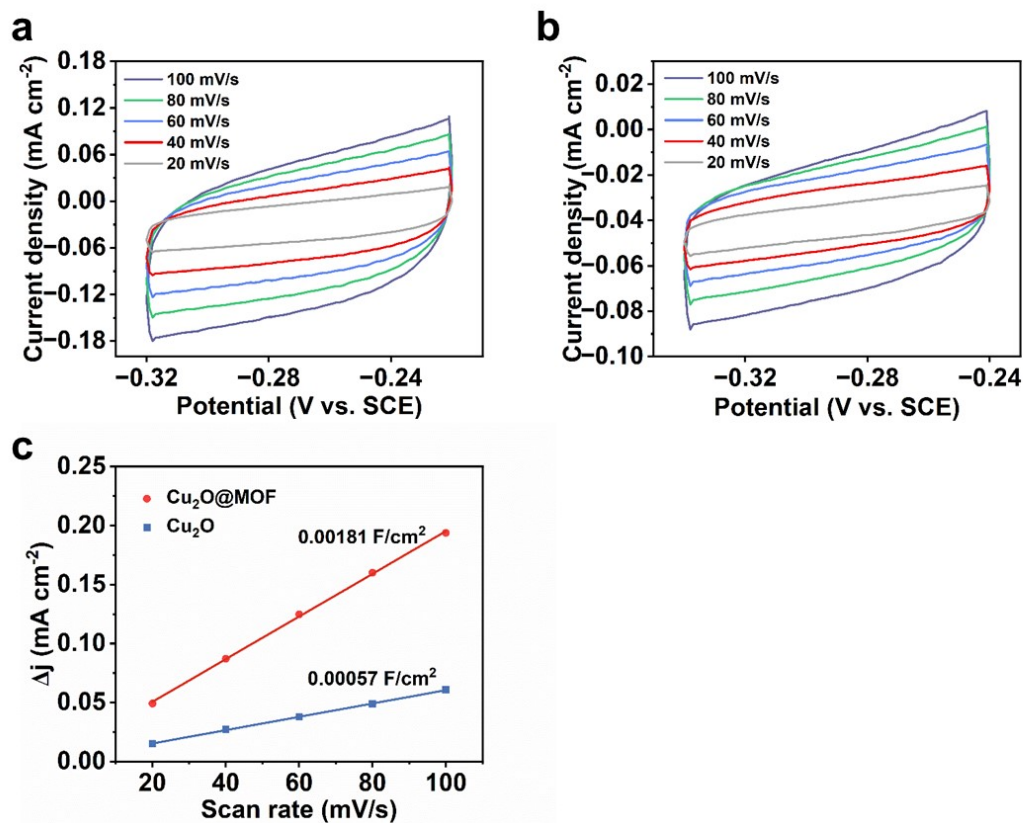


Fig. S17 Determination of the electrochemical active surface area (ECSA) by measuring the double-layer capacitance from cyclic voltammograms obtained at various scan rate (20, 40, 60, 80, 100 mV/s). a) Cu_2O ; b) $\text{Cu}_2\text{O}@MOF$. c) The double-layer capacitances of Cu_2O and $\text{Cu}_2\text{O}@MOF$.

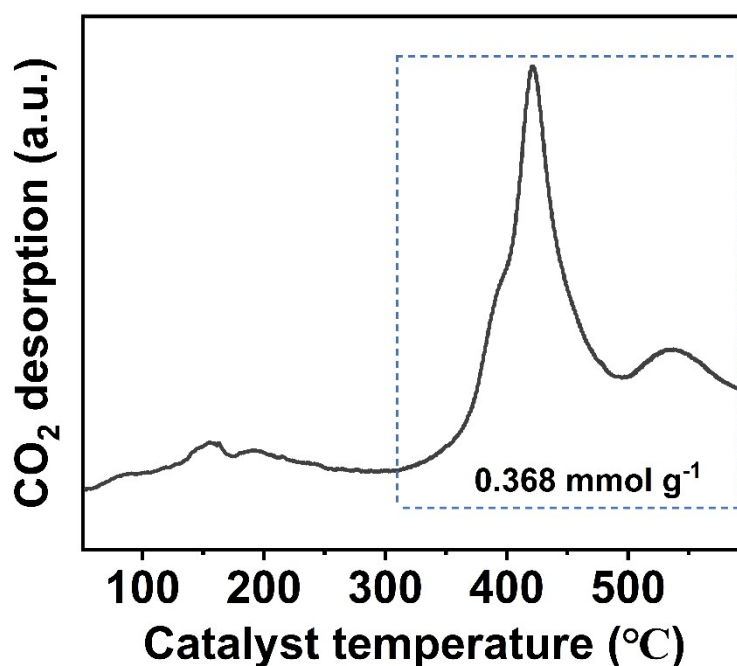


Fig. S18 The experimental CO₂-TPD profile of Cu₂O@MOF. The active sites involved in the reaction was determined by CO₂ chemisorption with a Micromeritics AutoChem II 2920 instrument. A weighed sample of the catalyst was inserted in the quartz tube. The sample was heated from room temperature to 600 °C at 10 °C min⁻¹ for pretreatment. After line cleaning with helium flow (30 mL min⁻¹) for 1 h, followed by cooling to 50 °C. A CO₂/He mixture (30 mL min⁻¹) was injected for 1 h until saturation, and then helium flow (30 mL min⁻¹) was switched and purged for 1 h to remove weakly physically adsorbed CO₂ on the surface. Finally, the desorption was carried out under the helium atmosphere at a temperature ramping rate of 10 °C/min up to 600 °C. The molar amount of chemisorbed CO₂ per mass of catalyst (mmol g_{cat}⁻¹) was calculated by integrating the peak area, which was calculated as 0.368 mmol g_{cat}⁻¹. The mass-based site density (SD) with CO₂ chemisorption was then calculated via Avogadro's constant (N_A , 6.02×10^{23} mol⁻¹) according to

$$SD(CO_2) = nCO_2 \times N_A \times 10^{-3}$$

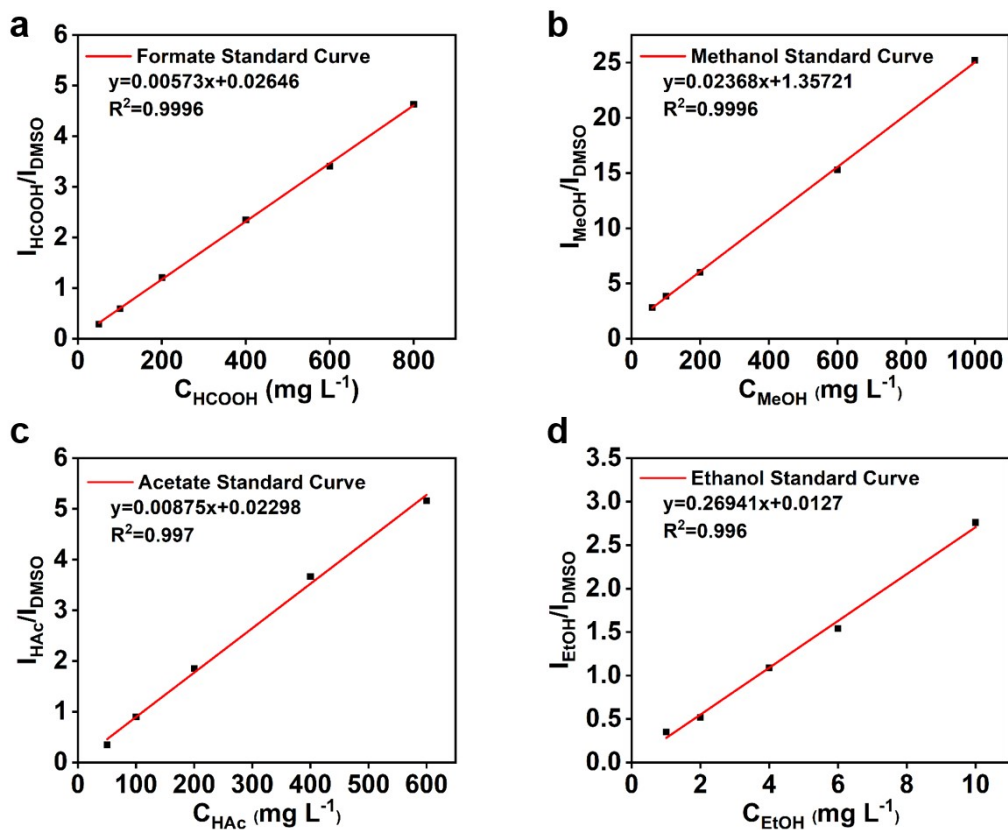


Fig. S19 The concentration standard curves of a) formate, b) methanol, c) acetate and d) ethanol. Calibration curve plots the ratio of integration area between target chemicals and internal standard DMSO versus the concentration of targets in standard solutions.

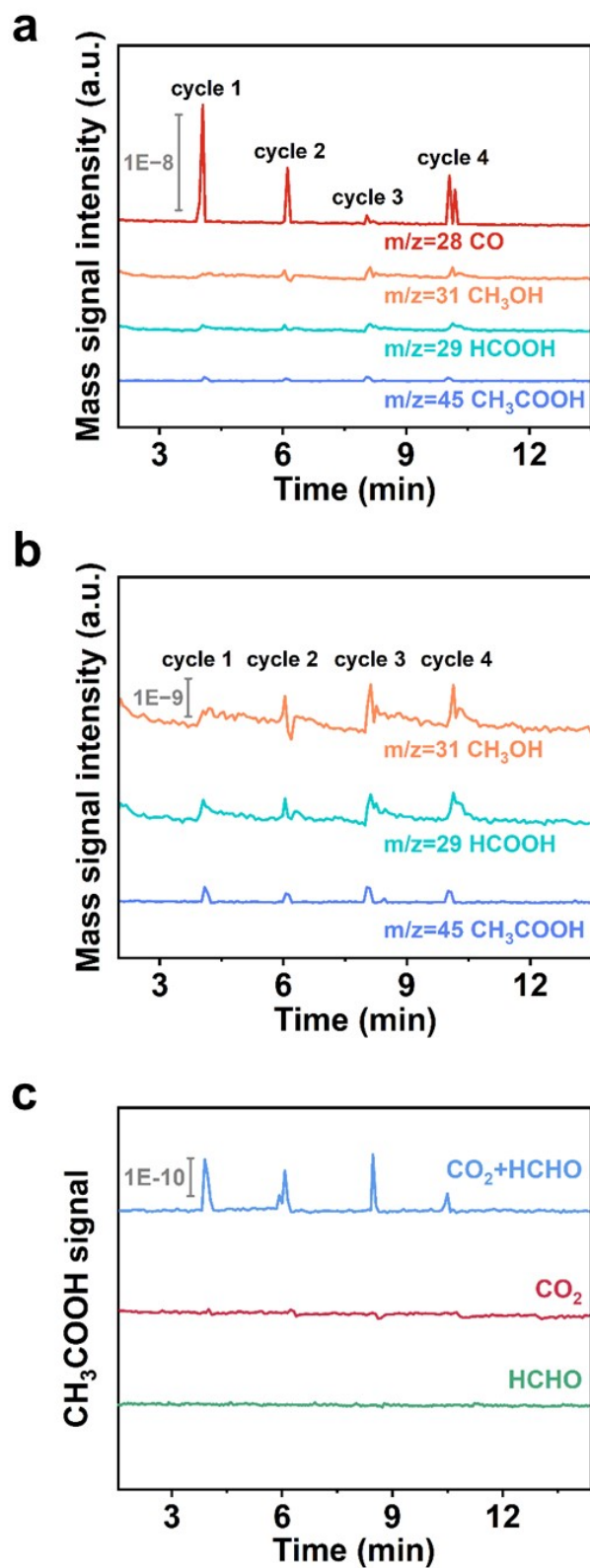


Fig. S20 a) Online DEMS measurements for the co-electrolysis of CO₂ and HCHO over Cu₂O@MOF composite. b) Magnification of selected DEMS signals in a). c) Online DEMS spectra of CH₃COOH signals over Cu₂O@MOF.

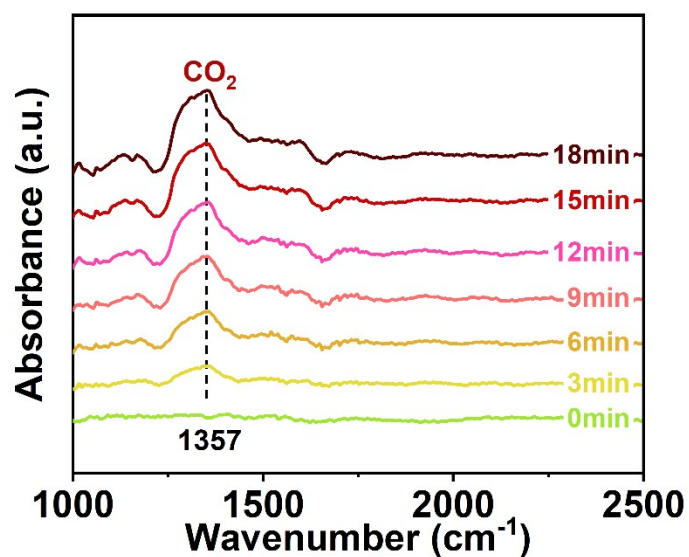


Fig. S21 FT-IR detection of adsorbed CO₂ on Cu₂O@MOF.

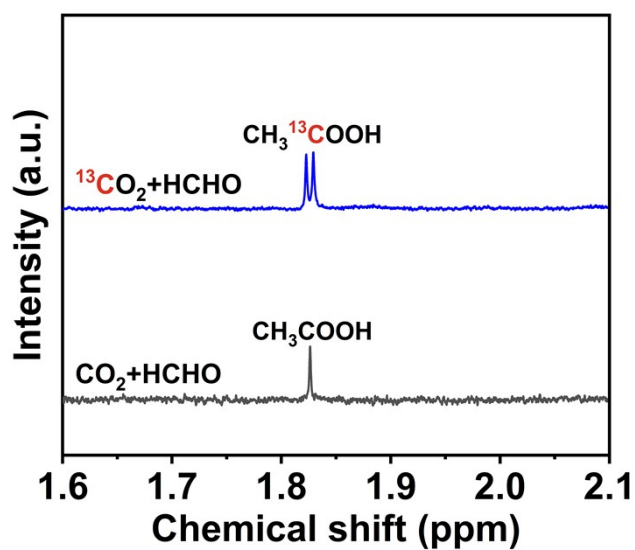


Fig. S22 ¹H NMR spectra of the liquid-phase products from electrocatalytic HCHO coupling with ¹²CO₂ and isotope-labelled ¹³CO₂.

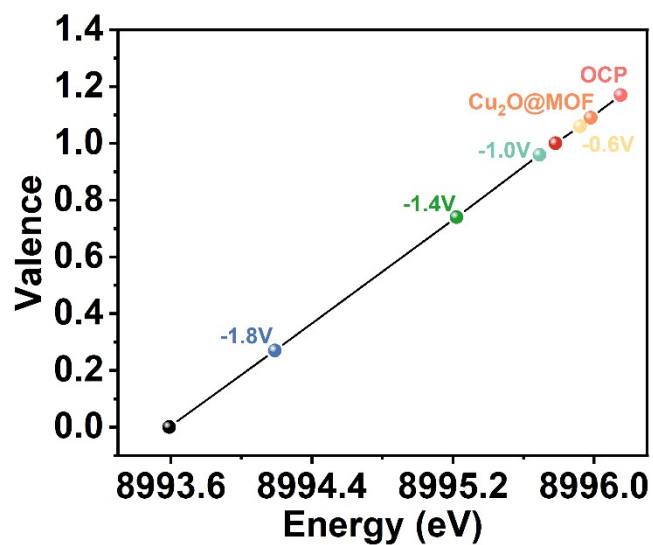


Fig. S23 The oxidation state analysis by edge position fitting of XANES of as-prepared Cu₂O@MOF in CO₂-saturated 1 M KOH solution containing 0.1 M HCHO at open circuit potential or different applied potentials.

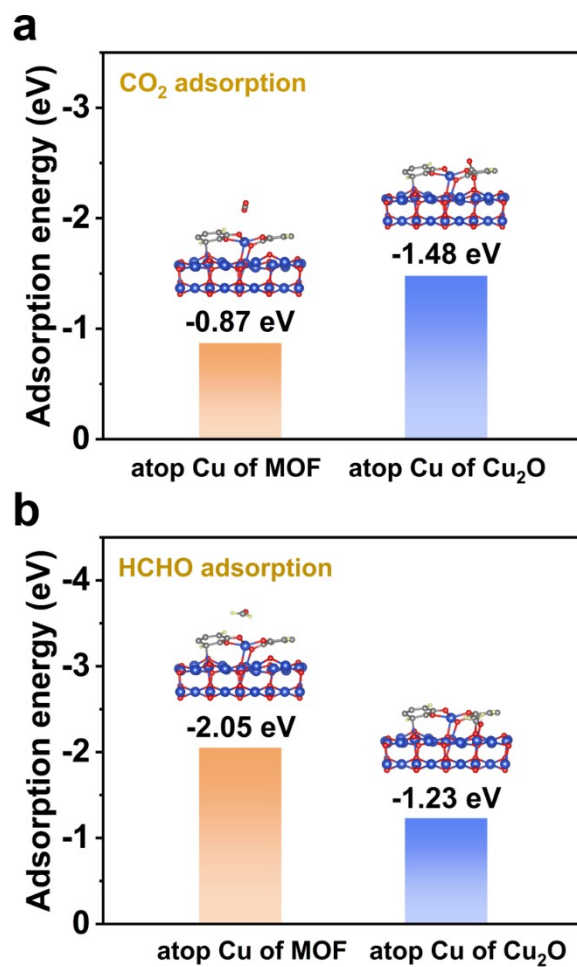


Fig. S24 The adsorption energy of (a) CO₂ and (b) HCHO on Cu sites of Cu-MOF and Cu₂O, respectively.

Table S1 Previous work on electrocatalytic production of acetate from CO/CO₂.

Catalyst	Carbon source	Mass of catalyst (mg cm ⁻²)	Current density (mA cm ⁻²)	Acetate productivity (mg L ⁻¹ h ⁻¹)	Characterization	Reference
Cu nanocube	CO	0.5	450	~3800	In situ Raman DFT	12
Cu nanoparticle	CO	0.5	200	950	LSV	13
Cu/Ag-DA	CO	0.2	100	2379	XAFS DFT In situ Raman	14
N-ND/Cu	CO ₂	/	<1	3.4	DFT	15
Mo ₈ @Cu/TNA	CO ₂	/	110	375	XAFS DFT	16
Mn-Cor-CP	CO ₂	0.5	0.8	4.68	NMR FTIR	17
SW-Cu(OH) ₂ /Cu	CO ₂	/	121.4	300	In situ Raman	18
NDD _L /Si RA	CO ₂	/	<1	96.1	In situ IR	19
PcCu-TFPN	CO ₂	0.5	12.5	/	In situ FTIR XAFS DFT	20
Cu ₂ O@MOF	CO ₂ +HCHO	1	154	654		This work
Cu ₂ O@MOF	CO ₂ +HCHO	1	13.4	72	In situ IR XAFS DFT DEMS In situ IR	This work (liquid-phase)

Table S2 The amounts of methanol and formate contributed by Cannizzaro reaction and the reduction of CO₂/HCHO in MEA electrolyzer.

Cell voltage	nHCOOH (mmol)		nCH ₃ OH (mmol)	
	From Cannizzaro reaction	From CO ₂ electroreduction	From Cannizzaro reaction	From electroreduction
-3.4 V	0.1	0.94	0.1	3.63
-3.6 V	0.07	1.11	0.07	4.76
-3.8 V	0.09	0.91	0.09	2.92
-4.0 V	0.04	1.07	0.04	3.69
-4.2 V	0.09	0.69	0.09	5.65

To evaluate and exclude the contribution of Cannizzaro reaction in the quantification of formate and methanol production, control experiments were conducted to obtain the amount of HCOOH and CH₃OH from Cannizzaro reaction. At a cell voltage of -3.4 to -4.2 V, N₂ instead of CO₂ was fed into the cathode chamber along with formaldehyde, and after one hour of reaction, samples were collected from both the cathode stream and anolyte for NMR tests. At the reduction potential, the amount of HCOOH detected can be assigned to Cannizzaro reaction instead of HCHO electrooxidation, which is the same as that of CH₃OH from Cannizzaro reaction. Thus, the production of HCOOH from CO₂ electroreduction and CH₃OH from the electroreduction of reactants can be calculated by subtracting the contributions of Cannizzaro reaction from the overall side-products.

Table S3 The amounts of methanol and formate contributed by Cannizzaro reaction and the reduction of CO₂/HCHO in H-type cell.

Potential vs. SCE	nHCOOH (mmol)		nCH ₃ OH (mmol)	
	From Cannizzaro reaction	From CO ₂ electroreduction	From Cannizzaro reaction	From electroreduction
-1.0 V	0.27	0.03	0.27	0.07
-1.2 V	0.34	0.11	0.34	0.29
-1.4 V	0.32	0.12	0.32	0.33
-1.6 V	0.29	0.17	0.29	0.81
-1.8 V	0.30	0.23	0.30	1.87

Electrolysis was performed in a two-compartment electrochemical cell using Cu₂O@MOF as the working electrode at different potentials, where 1 M KOH with 0.1 M HCHO was used as the catholyte and 1 M KOH as the anolyte.

References

- 1 Y. Zhou, Y. Yao, R. Zhao, X. Wang, Z. Fu, D. Wang, H. Wang, L. Zhao, W. Ni, Z. Yang, Y.-M. Yan, *Angew. Chem. Int. Ed.*, 2022, **61**, e202205832.
- 2 W. Cheng, H. Zhang, D. Luan, X. W. Lou, *Sci. Adv.*, 2021, **7**, eabg2580.
- 3 R. K. Miao, Y. Xu, A. Ozden, A. Robb, C. P. O'Brien, C. M. Gabardo, G. Lee, J. P. Edwards, J. E. Huang, M. Fan, X. Wang, S. Liu, Y. Yan, E. H. Sargent, D. Sinton, *Joule*, 2021, **5**, 2742-2753.
- 4 Y. Wu, Z. Jiang, Z. Lin, Y. Liang and H. Wang, *Nat. Sustain.*, 2021, **4**, 725-730.
- 5 G. Kresse, J. Furthmüller, *Comput. Mater. Sci.*, 1996, **6**, 15-50.
- 6 G. Kresse, J. Furthmüller, *Phys. Rev. B*, 1996, **54**, 11169-11186.
- 7 J. P. Perdew, K. Burke, M. Ernzerhof, *Phys. Rev. Lett.*, 1996, **77**, 3865-3868.
- 8 G. Kresse, D. Joubert, *Phys. Rev. B*, 1999, **59**, 1758-1775.
- 9 P. E. Blöchl, *Phys. Rev. B*, 1994, **50**, 17953-17979.
- 10 S. L. Dudarev, G. A. Botton, S. Y. Savrasov, C. J. Humphreys, A. P. Sutton, *Phys. Rev. B*, 1998, **57**, 1505-1509.
- 11 S. Grimme, J. Antony, S. Ehrlich, H. Krieg, *J. Chem. Phys.*, 2010, **132**, 154104.
- 12 P. Zhu, C. Xia, C.-Y. Liu, K. Jiang, G. Gao, X. Zhang, Y. Xia, Y. Lei, H. N. Alshareef, T. P. Senftle, H. Wang, *Proc. Natl. Acad. Sci. U.S.A.*, 2021, **118**, e2010868118.
- 13 S. Overa, B. S. Crandall, B. Shrimant, D. Tian, B. H. Ko, H. Shin, C. Bae, F. Jiao, *Nat. Catal.*, 2022, **5**, 738-745.
- 14 J. Jin, J. Wicks, Q. Min, J. Li, Y. Hu, J. Ma, Y. Wang, Z. Jiang, Y. Xu, R. Lu, G. Si, P. Papangelakis, M. Shakouri, Q. Xiao, P. Ou, X. Wang, Z. Chen, W. Zhang, K. Yu, J. Song, X. Jiang, P. Qiu, Y. Lou, D. Wu, Y. Mao, A. Ozden, C. Wang, B. Y. Xia, X. Hu, V. P. Dravid, Y.-M. Yiu, T.-K. Sham, Z. Wang, D. Sinton, L. Mai, E. H. Sargent, Y. Pang, *Nature*, 2023, **617**, 724-729.
- 15 H. Wang, Y.-K. Tzeng, Y. Ji, Y. Li, J. Li, X. Zheng, A. Yang, Y. Liu, Y. Gong, L. Cai, Y. Li, X. Zhang, W. Chen, B. Liu, H. Lu, N. A. Melosh, Z.-X. Shen, K. Chan, T. Tan, S. Chu, Y. Cui, *Nat. Nanotechnol.*, 2020, **15**, 131-137.
- 16 D. Zang, Q. Li, G. Dai, M. Zeng, Y. Huang, Y. Wei, *Appl. Catal. B: Environ.*, 2021, **281**, 119426.
- 17 R. De, S. Gonglach, S. Paul, M. Haas, S. S. Sreejith, P. Gerschel, U.-P. Apfel, T. H. Vuong, J. Rabeah, S. Roy, W. Schöfberger, *Angew. Chem. Int. Ed.*, 2020, **59**, 10527-10534.

- 18 J. Li, Y. Kuang, X. Zhang, W.-H. Hung, C.-Y. Chiang, G. Zhu, G. Chen, F. Wang, P. Liang, H. Dai, *Nat. Catal.*, 2023, **6**, 1151-1163.
- 19 Y. Liu, S. Chen, X. Quan, H. Yu, *J. Am. Chem. Soc.*, 2015, **137**, 11631-11636.
- 20 X.-F. Qiu, J.-R. Huang, C. Yu, Z.-H. Zhao, H.-L. Zhu, Z. Ke, P.-Q. Liao, X.-M. Chen, *Angew. Chem. Int. Ed.*, 2022, **61**, e202206470.